THE JOURNAL OF PHYSICAL CHEMISTRY C

Article

pubs.acs.org/JPCC

STM Imaging of Three-Metal-Center Molecules: Comparison of Experiment and Theory For Two Mixed-Valence Oxidation States

Natalie A. Wasio,[†] Rebecca C. Quardokus,[†] Ryan P. Forrest,[†] Steven A. Corcelli,[†] Yuhui Lu,[‡] Craig S. Lent,[§] Frederic Justaud,[∥] Claude Lapinte,[∥] and S. Alex Kandel*,[†]

[†]Department of Chemistry and Biochemistry, University of Notre Dame, Notre Dame, Indiana 46556, United States

[‡]Department of Chemistry, Louisiana College, Pineville, Louisiana 71360, United States

[§]Department of Engineering, University of Notre Dame, Notre Dame, Indiana 46556, United States

[∥]UMR CNRS 6226 Institut des Sciences Chimiques de Rennes, Université de Rennes I, 35042 Rennes Cedex, France

ABSTRACT: The molecule {Cp*(dppe)Fe(C≡C−)}$_3$(1,3,5-C$_6$H$_3$) (Fe3) was adsorbed on a single-crystal gold surface and studied using ultrahigh-vacuum scanning tunneling microscopy (STM). Both the singly oxidized Fe3$^+$ and doubly oxidized Fe3^{2+} are mixed-valence ions, and localization of the charge at specific metal centers was observed as the appearance of pronounced asymmetry in STM images. Switching the tip−sample bias voltage demonstrates that this asymmetry is electronic in nature. The nature of intramolecular structure and the degree of asymmetry produced in STM images varies according to the state of the scanning tip. Constrained density functional theory was used to simulate STM images for the neutral molecule and for both mixed-valence species, and simulated images agreed closely with observed results. In particular, changing the number of molecular electronic states contributing to contrast in the STM image produced a good match to the variation in structures measured experimentally.

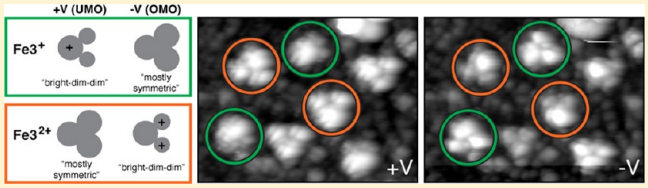

INTRODUCTION

Molecules with mixed-valence oxidation states are compelling targets of study. These molecules provide important model systems for intramolecular charge transfer,[1,2] and their electronic and optical properties are of potential use in materials and devices.[3,4] Our own interest in mixed-valence molecules stems from the possibility of exploiting their charge-transfer properties to create molecular components usable in electronic devices based upon the quantum cellular automata (QCA) architecture.[5−12]

Previous reports from our laboratory have described scanning tunneling microscopy (STM) imaging of mixed-valence molecules, and compared the STM images to the results of electronic-structure calculations.[13,14] Most recently, we showed that a geometry difference in a central benzene linker determined the degree of localization observed for single molecules. For two dinuclear organometallic molecules with identical Cp*Fe(dppe) metal−ligand systems, the meta compound showed localization of intramolecular charge that appeared as a bias-dependent "bright-dim" contrast in STM images, while the para-Fe2 compound showed delocalized charge and symmetric STM images.[15]

In this manuscript, we present STM images and constrained density-functional (CDFT) calculations of the trimetallic molecule Fe3, based on the same Cp*Fe(dppe) unit linked to the central benzene at the 1, 3, and 5 positions. A model of Fe3 is shown in Figure 1a,b. Like the meta-Fe2 molecule studied previously, we do not expect the π-electron system of the benzene to effectively couple the metal nuclei. Consequently, this molecule is a mixed-valence species in both the +1 and +2 charge states when studied in solution. The increased complexity of this molecule, and the correspondingly greater range of experimental images that can be acquired, provides a more stringent test of the theoretical models used. We present a detailed comparison between experiment and theory in this manuscript.

EXPERIMENTAL AND THEORETICAL METHODS

Neutral Fe3 and mixed-valence Fe3$^+$ and Fe3^{2+} were prepared and deposited in a similar manner as previously reported. Briefly, Fe3 was dissolved in tetrahydrofuran (THF), and stoichiometric quantities of FcPF$_6$ were added to produce the desired mixed-valence state or mixture of states. Solution was injected directly onto a vacuum-sputtered and annealed Au(111)-on-mica sample, and solvent was allowed to evaporate at room temperature. This preparation method has the advantages of being suitable to deposit virtually any molecule, and it does not break down the Fe3 species, which are both heat- and air-sensitive.[16,17]

We varied the extent of oxidation considerably over the course of many experiments, although for any given sample, the very small quantities of Fe3 used made the preparation of specific oxidation states somewhat imprecise. However, we were able to compare samples with neutral Fe3 to those

Received: November 12, 2012
Revised: November 16, 2012
Published: November 16, 2012

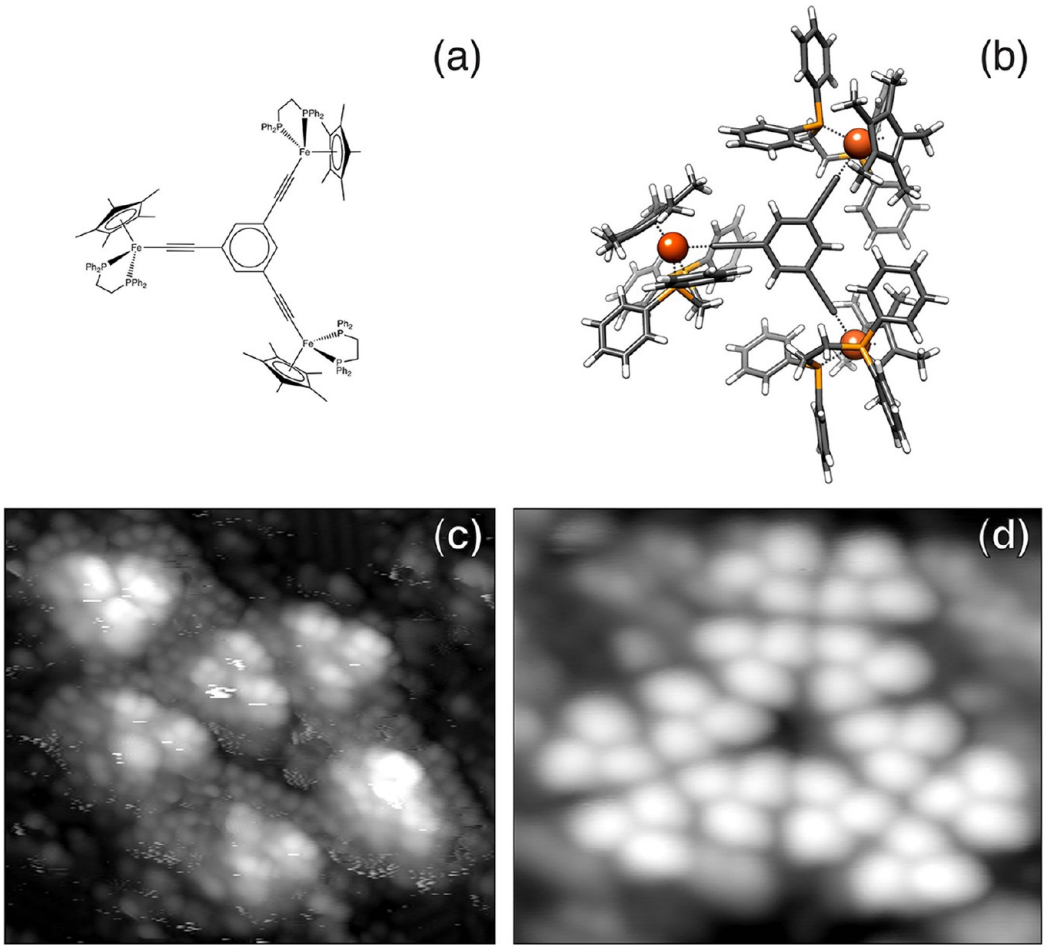

Figure 1. Structural formula (a) and model (b) of Fe3: $\{Cp^*(dppe)Fe(C{\equiv}C{-})\}_3(1,3,5\text{-}C_6H_3)$. The lower panels show STM images of neutral Fe3, (c) 106 Å × 94 Å, coadsorbed with solvent in relative disorder, imaged at +2 V bias; and (d) more closely packed, 91 Å × 74 Å, −1 V bias.

containing both Fe3 and $Fe3^+$, and both of the previous two samples containing $Fe3^+$ and $Fe3^{2+}$. By noting the similarities and differences between molecular features in these samples, we build up a reasonable degree of certainty that our samples do contain the oxidized species we are interested in studying.

STM images were acquired at 77 K with an ultrahigh-vacuum low-temperature STM (Omicron Nanotechnology LT-STM) using mechanically cut Pt/Ir tips. All images were acquired in constant-current mode at a current of 10 pA, in order to minimize the interaction of the tip with surface-adsorbed molecules. Other than image flattening to correct for surface tilt, all data presented are raw STM data, with no filtering or postprocessing performed.

Electronic structure calculations were performed using NWCHEM.[18] Density functional theory (DFT) was used for calculations performed on neutral Fe3. For mixed-valence systems such as $Fe3^+$ and $Fe3^{2+}$, traditional DFT has been shown to be inadequate because it most often delocalizes the charge.[19] For this reason, the calculations performed on $Fe3^+$ and $Fe3^{2+}$ instead used CDFT.[20] CDFT overcomes the delocalization problem by calculating the electron density subject to a charge constraint applied to a set of atoms.[21−23]

The B3LYP exchange-correlation functional was utilized for all DFT and CDFT calculations with the 6-311G(d, p) basis set for C, H, and P atoms and the LANL2TZ(f) effective core potential basis set for Fe atoms. Calculations were performed on the full Fe3 molecule with atomic positions taken directly from published X-ray crystallographic data[24] as well as an Fe3 molecule with simplified ligands. The ligands were simplified in accordance with previous studies which replaced all dppe and Cp* ligands with pairs of PH_3 and Cp ligands respectively.[14,15] For the CDFT calculations positive unit charges were constrained to entire $Cp^*Fe(dppe)(C{\equiv}C{-})$ or simplified $CpFe(PH_3)_2(C{\equiv}C{-})$ moieties.

RESULTS AND DISCUSSION

Neutral Fe3. Figure 1c,d shows STM images of neutral Fe3 on Au(111): the sample imaged in panel a was prepared using Fe3 only, while the image in panel b was selected from a sample where $Fe3^+$ (discussed in the following section) was also coadsorbed, though not imaged here. Molecular features consist of three bright, symmetric lobes concentrated around the iron-ligand centers. This is consistent with Fe3 molecules that adsorb with the plane of the molecule mostly flat on the surface, and, as all iron atoms are in the +2 oxidation state, each Fe3 molecule appears symmetric in these STM images. 3-fold symmetry was observed for all neutral Fe3 molecules across multiple experiments, regardless of the state of the STM tip. Rather more variation was observed in the relative order of surfaces prepared, with some experiments producing loosely aggregated, disordered Fe3 molecules with a range of intermolecular spacings, and others (panel d of Figure 1) showing closer packing and increased order. This is presumably due to the complex and variable nature of the solvent-drying

dx.doi.org/10.1021/jp311203u | J. Phys. Chem. C 2012, 116, 25486−25492

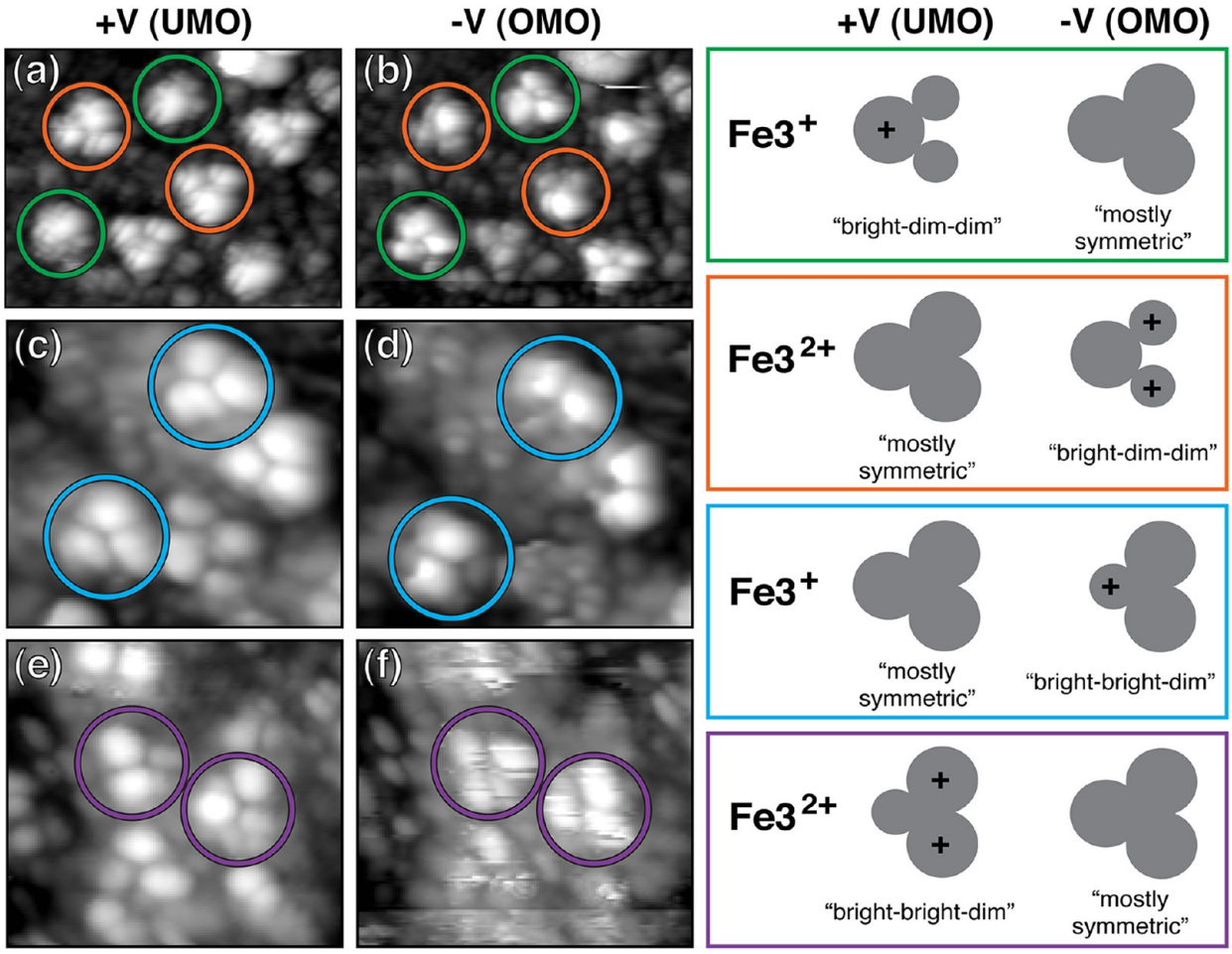

Figure 2. Images of samples containing an equal mixture of $Fe3^{+}$ and $Fe3^{2+}$, acquired at positive sample bias (panels a, c, and e) and negative sample bias (panels b, d, and f). Intramolecular contrast depends on the state of the tip for both $Fe3^{+}$ (green and blue) and $Fe3^{2+}$ (orange and purple). Panels a and b were acquired at ±2 V and are 145 Å × 111 Å; panels c–f were acquired at ±1 V and are 42 Å × 38 Å.

process in vacuum. In almost all images, we observe smaller and dimmer structures that can be attributed to solvent molecules or to the $FcPF_6$ oxidant, coadsorbed along with Fe3 species. We have run a number of control experiments depositing solutions with different components absent or present, in order to confirm these assignments.[14−16]

Mixed-Valence $Fe3^{+}$ and $Fe3^{2+}$. According to the Robin−Day classification, Fe3 is considered a Class II mixed-valence complex; that is, intramolecular electron transfer between metal centers is slow.[25] Potentially, charge localized within a mixed-valence complex will appear as an asymmetric electron density in an STM image. This was observed for the Class II meta-Fe2 compound, which shares with Fe3 the 1,3-substituted geometry around the central benzene.[15]

Figure 2 shows samples with mixed-valence species, prepared to be an equal mixture of singly oxidized $Fe3^{+}$ and doubly oxidized $Fe3^{2+}$. Images were acquired at both positive and negative junction bias to allow for a more sensitive probe of electronic structure.[26,27] At positive sample biases, electrons tunnel from the tip to the sample, and image contrast is influenced more significantly by unoccupied molecule-surface electronic states; conversely, negative sample biases induce tunneling from the sample to the tip and reveal occupied molecule-surface electronic states.

A variety of molecular features appear in these images. Features circled in green appear asymmetric in the positive-bias image (Figure 2a), with two of the three lobes in the feature significantly dimmer than the third. (We note that the different orientation of these features implies that the asymmetry does not result from the microstructure of the STM tip.) In the negative-bias image (Figure 2b), these features appear largely symmetric. The opposite behavior is seen for the features circled in orange, which are largely symmetric at positive bias voltages, and appear as asymmetric, bright−dim−dim features at negative bias. Most molecular features were similar to the orange-circled or green-circled features in their appearance and bias-voltage dependence, although a minority of observed structures (viz., the molecule in the lower middle-left of the figure) appeared dissimilar to either. This may be the result of minor impurities in the sample, differences in adsorption geometry, or comproportionation to produce other Fe3 oxidation states.

Assigning features in STM images to molecules must be done cautiously. Qualitatively, we expect an $Fe3^{+}$ molecule to show an enhancement in empty electronic states and a corresponding depletion in filled electronic states, both appearing on only one of its three lobes. The green-circled features match this empty-state behavior (a), but appear relatively symmetric with respect to filled states (b), and we assign these features as $Fe3^{+}$. The orange-circled features are $Fe3^{2+}$, and while they appear relatively symmetric in empty-state density, they show depletion in two of three lobes in the

dx.doi.org/10.1021/jp311203u | J. Phys. Chem. C 2012, 116, 25486−25492

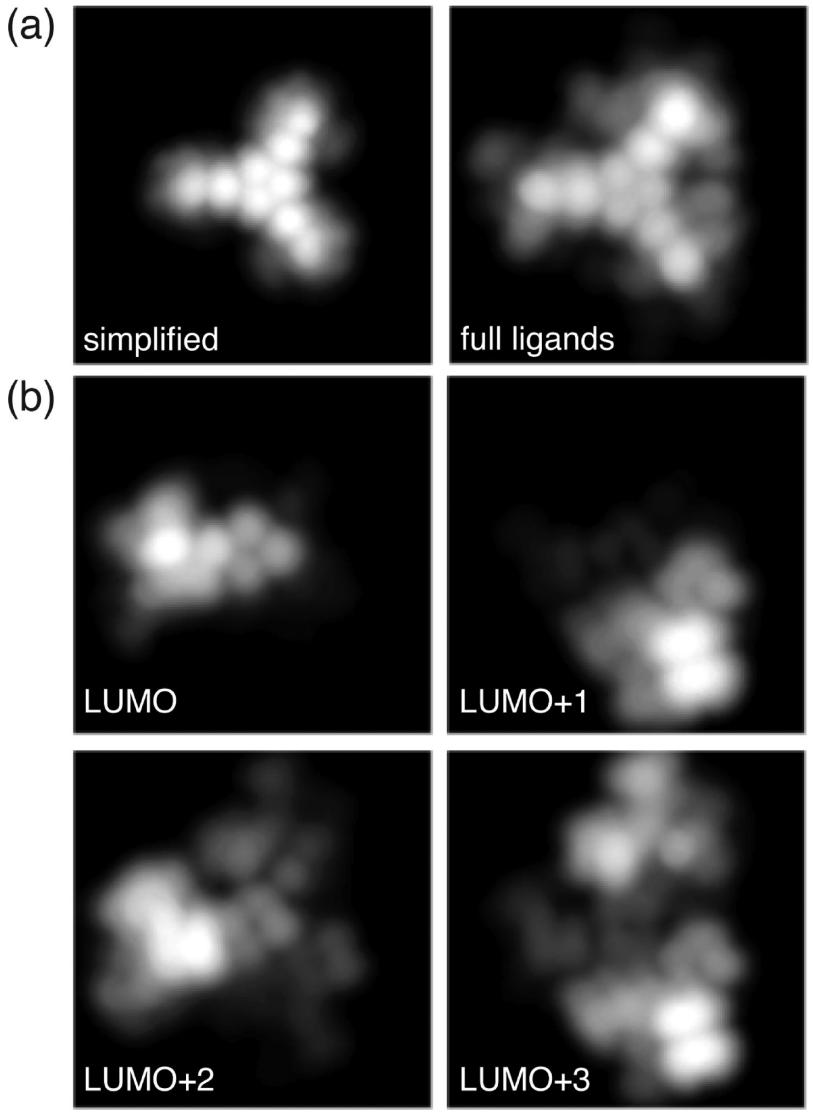

Figure 3. (a) Comparison of simulated STM images for neutral Fe3, using simplified ligands but optimized geometry, or full ligands but single-point geometry. (b) Calculated STM images for mixed-valence $Fe3^{+}$, broken down into contributions from individual electronic states, from LUMO through LUMO+3.

filled-state image. The sensitivity of STM images to variations in molecular electronic-state density will be discussed in more detail when comparing to theoretical calculations in the discussion.

We find that from experiment to experiment, the bias-dependent contrast in images of $Fe3^{+}$ and $Fe3^{2+}$ changes. This is demonstrated in Figure 2c–f, which shows additional images of these molecules, recorded under similar conditions but on different samples and different days. In these images, we observe $Fe3^{+}$ molecules where contrast is sharp in filled states, but empty-state features appear nearly symmetric (blue circles), as well as Fe^{2+} features showing high asymmetry in empty state images (purple circles.) Some molecular mobility obscures the $Fe3^{2+}$ features in Figure 2f, though they appear significantly more symmetric than the molecular features at positive bias. It is not uncommon for the state of the STM tip to affect the contrast observed in STM images, an effect that has been attributed to the tip electronic state density determining which surface states contribute to tunneling.[28,29] We note that generally, features identified with green circles for $Fe3^{+}$ are paired with orange-circled $Fe3^{2+}$ (as in Figure 2a,b); and blue circles with purple circles. However, we have observed a green-purple pairing, which indicates that the contrast mechanism may be a more complex function of the state of the tip.

Calculated STM Images. There are a number of different methods for using electronic-structure calculations to simulate STM images.[21−23,30−34] For all of these techniques, however, there is a trade-off between accuracy and expense, as exact computation of the result of an STM experiment requires a full quantum-mechanical treatment of the combined molecule-surface-tip system. For large molecules, such as the one studied here, this calculation is prohibitively complex given current computational resources. Our approach here is to disregard both the surface and the STM tip, and thus limit the electronic-structure calculation to the molecule in vacuum.[35] We note that this is necessarily less general and less rigorous than an approach that includes the sample and tip in the calculation,[34,36−44] and will discuss below what can still be gained from a comparison between experiment and theory.

dx.doi.org/10.1021/jp311203u | J. Phys. Chem. C 2012, 116, 25486−25492

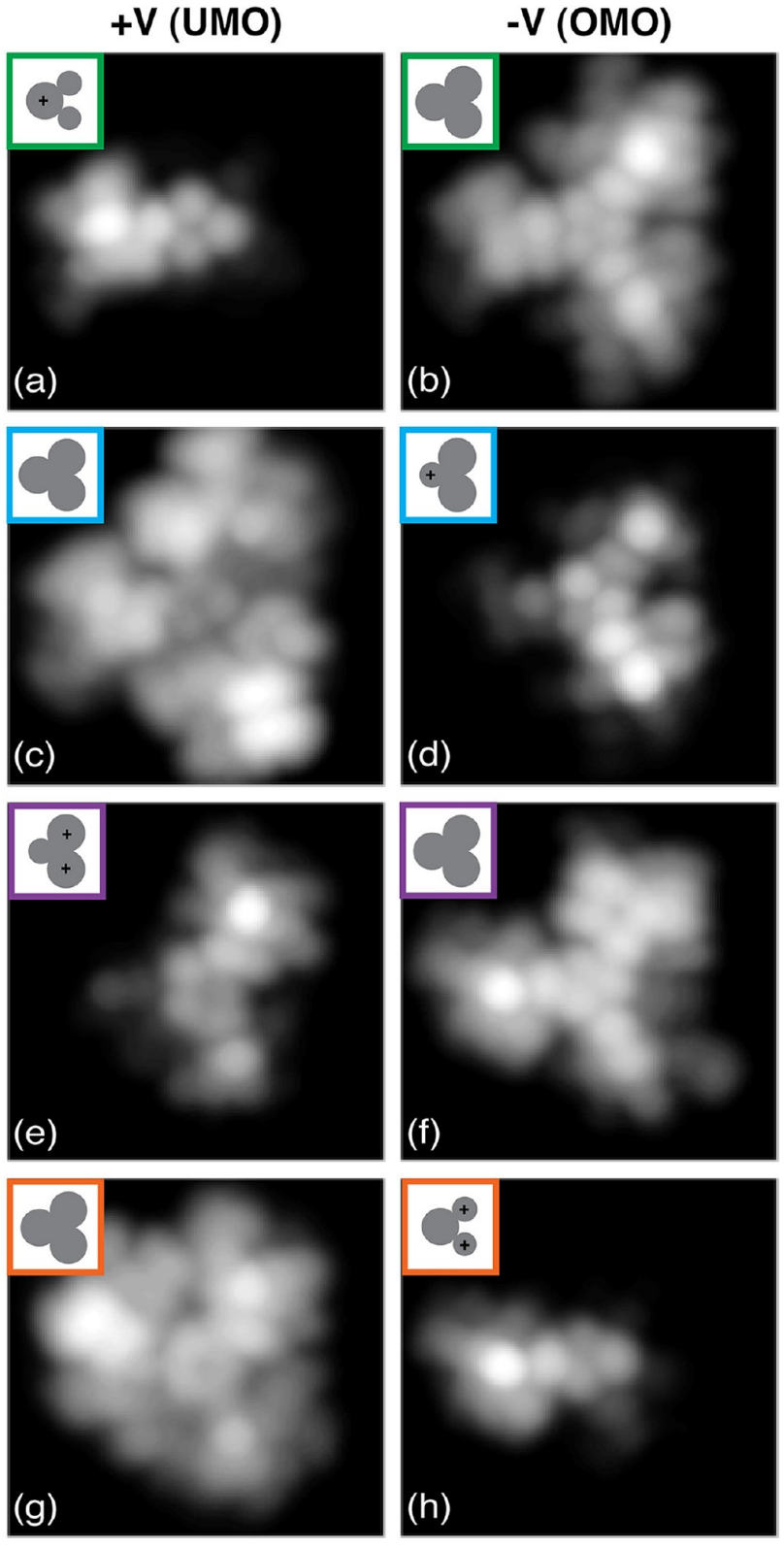

Figure 4. (a–d) Simulated STM images for mixed-valence $Fe3^{+}$. Green: LUMO at positive bias, HOMO through HOMO−4 at negative bias. Blue: LUMO through LUMO+4 at positive bias, HOMO at negative bias. (e–h) Simulated STM images for mixed-valence $Fe3^{2+}$. Purple: LUMO and LUMO+1 at positive bias, HOMO through HOMO−4 at negative bias. Orange: LUMO through LUMO+4 at positive bias, HOMO and HOMO−1 at negative bias.

The probability distributions that are the result of NWChem calculations are integrated over space to predict the tunneling current resulting from placing the STM tip at any given location. This integration is weighted, with the largest contribution to the tunneling current arising from the electron density in the vicinity of the tip, falling off exponentially with

dx.doi.org/10.1021/jp311203u | J. Phys. Chem. C 2012, 116, 25486–25492

distance. The decay constant of the exponential is an adjustable parameter. In the limit of short decay, this procedure maps out a surface of constant electron state density, while the long-decay limit projects the electron density onto two dimensions. Both of these limiting cases are established methods to simulate STM images. By selecting a decay length intermediate between these two limits, we aim for a more physically reasonable method for converting electron density distributions to tunneling current and, from there, STM images.

Figure 3a shows simulated STM images for neutral Fe3. The first simulation used a fully optimized molecular geometry, but simplified the diphenylphosphino ligands to pairs of PH_3 moieties. In contrast, a second simulation uses the full ligands, but did not employ a geometry optimization; instead, atomic positions were taken from published X-ray crystallographic data and used as-is. Because the geometry likely changes substantially on surface adsorption, there is no reason to think that a geometry optimized for the molecule in vacuum would be any more accurate than the experimental solid-state geometry.

While the image generated using the full dppe ligands shows intramolecular structure that is more complex, the two images are qualitatively similar in their overall symmetry and in the contrast between the center of the molecule and the outer lobes. In previous studies, we opted for simplified ligands to reduce computation time,[14,15] and Figure 3a bears out the reasonableness of that approach. In this manuscript, we opt to use the full ligands, without the computationally expensive step of optimizing the molecular geometry.

Experimental images of $Fe3^+$ and $Fe3^{2+}$ show a pronounced dependence on the sign of the tip−sample bias voltage; furthermore, the contrast evident in positive-bias and negative-bias images appears to change in some fashion with the state of the STM tip. To investigate this further, we construct images considering each calculated electronic state of $Fe3^+$ independently. These empty-state images for $Fe3^+$ are shown in Figure 3b. The asymmetry for the lowest unoccupied molecular orbital (LUMO), shown in panel (a), is qualitatively what one would expect: the metal−ligand system that is constrained to have one fewer electron shows up brightly compared to the other two iron centers. However, the experiment will be sensitive not only to the molecular LUMO, but also higher-lying empty states within the range of the bias voltage (1−2 V) applied between the tip and sample. Integration over multiple states will tend to produce images with more symmetric molecular features.

As we have already discussed, the contrast of $Fe3^+$ and $Fe3^{2+}$ changes according to the state of the STM tip, with two distinct features observed for each molecule. In general terms, each mixed-valence molecule shows asymmetry in its intramolecular contrast only at one tip−sample bias polarity: i.e., in Figure 2, both the $Fe3^+$ (green) and $Fe3^{2+}$ (purple) features are asymmetric at positive bias and symmetric at negative bias. Figure 4 presents simulated images for $Fe3^+$ and $Fe3^{2+}$ to which the experimental data can be compared. The best match for the green-and-purple coded images comes when the simulation assumes that only the LUMO contributes to positive-bias images, but that states ranging from the highest occupied molecular orbital (HOMO) to the HOMO−3 are important when imaging at negative bias. The other features observed for $Fe3^+$ and $Fe3^{2+}$ in Figure 2 are matched very well by the simulations colored blue and orange in Figure 4, which were calculated assuming that multiple electronic states (LUMO through LUMO+3) contribute at positive bias, while only the HOMO (and, for Figure 4h, the HOMO−1) are imaged at negative bias. The qualitative fit for both $Fe3^+$ and $Fe3^{2+}$ between Figure 2 and Figure 4 is excellent.

On a purely phenomenological basis, then, the experimental differences in tip contrast are explained by a shift in the Fermi level of the STM tip.[45−47] For example, a shift upward in the tip Fermi level would increase the number of unoccupied states imaged at positive bias, but narrow the number of occupied states imaged at negative bias. This is consistent with the shift from blue-coded to green-coded features for $Fe3^+$, or from orange to purple for $Fe3^{2+}$. A shift in the Fermi level of the tip relative to the sample could be either apparent or actual. Asymmetry in the tip density of states near the Fermi level could produce an apparent effect: if the tip microstructure determines whether the tip has a relatively greater number of filled or empty states, this could appear experimentally as a Fermi level shifted higher or lower.[45] Alternately, variations in the tip's chemical composition could result in an actual Fermi level shift. An additional possibility is that it is the sample Fermi level that is shifting relative to the tip. $Fe3^+$ and $Fe3^{2+}$ are typically imaged coadsorbed with, and potentially on top of, solvent molecules. Changing surface conditions could affect the adsorption environment, and in that way be responsible for the contrast differences observed.

Overall, qualitative agreement is quite strong between the experimentally observed images of $Fe3^+$ and $Fe3^{2+}$ and the images simulated using electronic-structure calculations of the molecules in vacuum. Agreement between experiment and calculation is excellent for this molecule as a neutral species and for two cationic oxidation states, and a similar approach produced good agreement for the previously observed Fe2 species.[14,15] It is noteworthy, and perhaps surprising, that a simplified calculation that ignores the effect of the surface and STM tip can nonetheless appear qualitatively correct. We do not expect that this approach would work similarly well for other molecules, for which a more general treatment would be necessary.[34,36−44] For Fe3, we suggest that a number of factors may be responsible for the in-vacuum calculation producing good results. First among these is the effect of the relatively bulky dppe ligands, which will tend to insulate the iron centers from the surface; previous experiments have shown that the presence of an intentionally adsorbed insulating layer may result in STM images that more closely resemble molecular frontier orbitals, and the ligands may serendipitously be playing a similar role. This effect could be magnified by the tendency for STM image contrast to depend strongly on the metal centers and much more weakly on the specifics of the ligand geometry, which would additionally explain why moderate changes in geometry on adsorption would not invalidate the comparison between experiment and a gas-phase calculation.

In conclusion, CDFT is effective for calculating STM images of mixed-valence molecules, and it reproduces relatively complex tip-dependent variation in intramolecular structure for the Fe3 mixed-valence system. Both $Fe3^+$ and $Fe3^{2+}$ ions are observed via STM to be asymmetric in their electronic structure, with stable, localized electronic state density consistent with their assignment as class II mixed-valence molecules.

AUTHOR INFORMATION

Corresponding Author

*E-mail: skandel@nd.edu.

Notes

The authors declare no competing financial interest.

■ ACKNOWLEDGMENTS

This work was supported by the National Science Foundation under NSF CHE-0848415 and NSF CHE-1124762.

■ REFERENCES

(1) Weyland, T.; Costuas, K.; Toupet, L.; Halet, J. F.; Lapinte, C. *Organometallics* **2000**, *19*, 4228−4239.
(2) Costuas, K.; Rigaut, S. *Dalton Trans.* **2011**, *40*, 5643−5658.
(3) Weyland, T.; Ledoux, I.; Brasselet, S.; Zyss, J.; Lapinte, C. *Organometallics* **2000**, *19*, 5235−5237.
(4) Ghazala, S. I.; Paul, F.; Toupet, L.; Roisnel, T.; Hapiot, P.; Lapinte, C. *J. Am. Chem. Soc.* **2006**, *128*, 2463−2476.
(5) Arima, V.; Iurlo, M.; Zoli, L.; Kumar, S.; Piacenza, M.; Della Sala, F.; Matino, F.; Maruccio, G.; Rinaldi, R.; Paolucci, F.; et al. *Nanoscale* **2012**, *4*, 813−823.
(6) Braun-Sand, S.; Wiest, O. *J. Phys. Chem. A* **2003**, *107*, 285−291.
(7) Tokunaga, K. *Phys. Chem. Chem. Phys.* **2009**, *11*, 1474−1483.
(8) Qi, H.; Sharma, S.; Li, Z.; Snider, G.; Orlov, A.; Lent, C.; Fehlner, T. *J. Am. Chem. Soc.* **2003**, *125*, 15250−15259.
(9) Li, Z.; Beatty, A.; Fehlner, T. *Inorg. Chem* **2003**, *42*, 5707−5714.
(10) Tokunaga, K. *Materials* **2010**, *3*, 4277−4290.
(11) Qi, H.; Gupta, A.; Noll, B.; Snider, G.; Lu, Y.; Lent, C.; Fehlner, T. *J. Am. Chem. Soc.* **2005**, *127*, 15218−15227.
(12) Lu, Y.; Lent, C. S. *Nanotechnology* **2008**, *19*, 1−11.
(13) Guo, S.; Kandel, S. A. *J. Phys. Chem. Lett.* **2010**, *1*, 420−424.
(14) Lu, Y. H.; Quardokus, R.; Lent, C. S.; Justaud, F.; Lapinte, C.; Kandel, S. A. *J. Am. Chem. Soc.* **2010**, *132*, 13519−13524.
(15) Quardokus, R. C.; Lu, Y. H.; Wasio, N. A.; Lent, C. S.; Justaud, F.; Lapinte, C.; Kandel, S. A. *J. Am. Chem. Soc.* **2012**, *134*, 1710−1714.
(16) Guo, S.; Kandel, S. A. *J. Chem. Phys.* **2008**, *128*, 014702.
(17) Grill, L.; Stass, I.; Rieder, K. H.; Moresco, F. *Surf. Sci.* **2006**, *600*, L143−L147.
(18) Valiev, M.; Bylaska, E. J.; Govind, N.; Kowalski, K.; Straatsma, T. P.; Van Dam, H. J. J.; Wang, D.; Nieplocha, J.; Apra, E.; Windus, T. L.; et al. *Comput. Phys. Commun.* **2010**, *181*, 1477−1489.
(19) Cohen, A. J.; Mori-Sanchez, P.; Yang, W. T. *Science* **2008**, *321*, 792−794.
(20) Kaduk, B.; Kowalczyk, T.; Van Voorhis, T. *Chem. Rev.* **2012**, *112*, 321−370.
(21) Wu, Q.; Van Voorhis, T. *Phys. Rev. A* **2005**, *72*, 024502.
(22) Wu, Q.; Van Voorhis, T. *J. Phys. Chem. A* **2006**, *110*, 9212−9218.
(23) Wu, Q.; Van Voorhis, T. *J. Chem. Theory Comput.* **2006**, *2*, 765−774.
(24) Weyland, T.; Lapinte, C.; Frapper, G.; Calhorda, M.; Halet, J.; Toupet, L. *Organometallics* **1997**, *16*, 2024−2031.
(25) Robin, M.; Day, P. *Adv. Inorg. Chem. Radiochem.* **1967**, *10*, 247−422.
(26) Comanici, K.; Buchner, F.; Flechtner, K.; Lukasczyk, T.; Gottfried, J.; Steinrueck, H.; Marbach, H. *Langmuir* **2008**, *24*, 1897−1901.
(27) Nieminen, J.; Lahti, S.; Paavilainen, S.; Morgenstern, K. *Phys. Rev. B* **2002**, *66*, 165421.
(28) Sautet, P. *Chem. Rev.* **1997**, *97*, 1097−1116.
(29) Hofer, W.; Redinger, J. *Philos. Mag. B* **1998**, *78*, 519−525.
(30) Bardeen, J. *Phys. Rev. Lett.* **1961**, *6*, 57−59.
(31) Cerda, J.; Van Hove, M.; Sautet, P.; Salmeron, M. *Phys. Rev. B* **1997**, *56*, 15885−15899.
(32) Krajci, M.; Hafner, J. *Phys. Rev. B* **2011**, *84*, 115410.
(33) Blanco, J. M.; Flores, F.; Pérez, R. *Prog. Surf. Sci.* **2006**, *81*, 403−443.
(34) Villagomez, C.; Zambelli, T.; Gauthier, S.; Gourdon, A.; Stojkovic, S.; Joachim, C. *Surf. Sci.* **2009**, *603*, 1526−1532.
(35) Pascual, J.; Gómez-Herrero, J.; Rogero, C.; Baró, A.; Sánchez-Portal, D.; Artacho, E.; Ordejón, P.; Soler, J. *Chem. Phys. Lett.* **2000**, *321*, 78−82.
(36) Bellec, A.; Ample, F.; Riedel, D.; Dujardin, G.; Joachim, C. *Nano Lett.* **2009**, *9*, 144−147.
(37) Cheng, Z.; Du, S.; Jiang, N.; Zhang, Y.; Guo, W.; Hofer, W.; Gao, H.-J. *Surf. Sci.* **2011**, *605*, 415−418.
(38) Guillermet, O.; Gauthier, S.; Joachim, C.; de Mendoza, P.; Lauterbach, T.; Echavarren, A. *Chem. Phys. Lett.* **2011**, *511*, 482−485.
(39) Guo, Q.; Huang, M.; Qin, Z.; Cao, G. *Ultramicroscopy* **2012**, *118*, 17−20.
(40) Kasaya, K.; Tabata, H.; Kawai, T. *Surf. Sci.* **1998**, *406*, 302−311.
(41) Korventausta, A.; Paavilainen, S.; Niemi, E.; Nieminen, J. *Surf. Sci.* **2009**, *603*, 437−444.
(42) Soe, W.; Manzano, C.; De Sarkar, A.; Chandrasekhar, N.; Joachim, C. *Phys. Rev. Lett.* **2009**, *102*, 107102.
(43) Makoudi, Y.; Palmino, F.; Duverger, E.; Arab, M.; Cherioux, F.; Ramseyer, C.; Therrien, B.; Tschan, M. J. L.; Suess-Fink, G. *Phys. Rev. Lett.* **2008**, *100*, 076405.
(44) Repp, J.; Meyer, G.; Stojkovic, S.; Gourdon, A.; Joachim, C. *Phys. Rev. Lett.* **2005**, *94*, 026803.
(45) Pelz, J. *Phys. Rev. B* **1991**, *43*, 6746−6749.
(46) Passoni, M.; Donati, F.; Bassi, A. L.; Casari, C. S.; Bottani, C. E. *Phys. Rev. B* **2009**, *79*, 045404.
(47) Kwapinski, T.; Jalochowski, M. *Surf. Sci.* **2010**, *604*, 1752−1756.